Lanthanide-Based Coordination Polymers with a 4,5-Dichlorophthalate Ligand Exhibiting Highly Tunable Luminescence Toward Luminescent Bar Codes

Albert-Manga Badiane, Stéphane Freslon, Carole Daiguebonne, Yan Suffren, Kevin Bernot, Guillaume Calvez, Karine Costuas, Magatte Camara, Olivier Guillou

Lanthanide-Based Coordination Polymers With 4,5-Dichlorophthalate Ligand Exhibiting Highly Tunable Luminescence: Toward Luminescent Bar Codes.

Albert-Manga Badiane[b], Stéphane Freslon[a], Carole Daiguebonne[a,*], Yan Suffren[a,*], Kevin Bernot[a], Guillaume Calvez[a], Karine Costuas[a], Magatte Camara[b] and Olivier Guillou[a].

[a] Univ Rennes, INSA Rennes, CNRS, ISCR "Institut des Sciences Chimiques de Rennes", F-35708 Rennes.

[b] LCPM – Groupe "Matériaux Inorganiques: Chimie Douce et Cristallographie" Université Assane Seck de Ziguinchor, BP 523 Ziguinchor, Sénégal.

* To whom correspondence should be addressed.

ABSTRACT

Reaction in water of 4,5-dichlorophthalate ($dcpa^{2-}$) with the heaviest lanthanide ions leads to a family of compounds with general chemical formula $[Ln_2(dcpa)_3(H_2O)_5 \cdot 3H_2O]_\infty$ where $Ln = Tb-Lu$ plus Y. Synthesis, crystal structure, thermal behavior and luminescent properties of this series of homo-nuclear compounds are described. Additionally, this family can be extended to iso-structural hetero-nuclear compounds that can contain some light lanthanide ions and therefore present some original photo-physical properties. These compounds show potential interest as multi-emissive material (visible and infrared light between 450 and 1600 nm) and could find their application as luminescent bar-code.

KEYWORDS

INTRODUCTION

For more than a decade, there is a growing interest for lanthanide-based coordination compounds, particularly because of their interesting optical properties.[1-6] Our group, which is involved in that field for almost twenty years,[7] currently focuses its attention on luminescent hetero-lanthanide coordination polymers[8-11] that could be used as taggants for fight against counterfeiting.[12-14] Evidently, because technological applications are targeted, ligands must be commercially available, low cost, thermally stable and non-toxic. Moreover, the production process must be respectful of environment. Therefore we have investigated numerous benzene-poly-carboxylate ligands in association with lanthanide ions[8, 15-18] aiming bright and highly tunable luminescence. In the frame of this study, we have investigated lanthanide-based coordination polymers with 4,5-dichlorophthalate as ligand (Scheme 1).
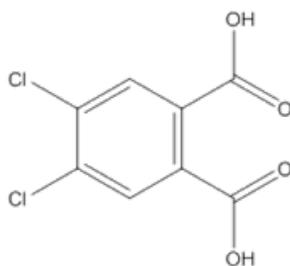
Scheme 1. Schematic representation of the 4,5-dichlorophthalic acid (4,5-dichlorobenzene-1,2-dicarboxylic acid) hereafter symbolized by $H_2(dcpa)$.

To the best of our knowledge, there is no lanthanide-based coordination polymer with this ligand reported so far.[19-20] Moreover, it has been demonstrated that the presence of a substituent on the phenyl ring hardly affects luminescent properties of lanthanide-based coordination polymers.[16-17] At last, chlorinated ligands are well known for their efficiency as flame retardant which could constitute an asset for technological applications.[21]

EXPERIMENTAL SECTION

Synthesis and characterization of the ligand

4,5-dichlorophthalic acid has been purchased from TCI (98 %) and used without further purification. It has been re-crystallized in water and its crystal structure has been solved. Crystal and final structure refinement data are listed in Table S1. A projection view of an asymmetric unit is drawn in Figure S1.

Two equivalent of sodium hydroxide were added to an aqueous suspension of 4,5-dichlorophthalic acid. Resulting clear solution was evaporated to dryness and the solid residue dissolved in ethanol and refluxed for one hour for insuring complete dissolution of impurities. Precipitation was provoked by addition of ethoxyethane. The obtained solid was filtered and dried under ambient conditions. Yield was about 90 %. By re-crystallization, single crystals of $Na_2(dcpa) \cdot 4H_2O$ suitable for X-ray diffraction were obtained. Crystal and final structure refinement data are listed in Table S2. A projection view of an asymmetric unit is drawn in Figure S2.

Comparison between the simulated powder diffraction pattern from this crystal structure and experimental powder diffraction diagram of the microcrystalline powder evidences that the microcrystalline powder and the single crystals are isostructural (Figure S3). This is supported by the thermal analysis of the microcrystalline powder (Figure S4) that shows the departure of four water molecules per formula.

Chemical analysis for $Na_2(dcpa) \cdot 4H_2O$ ($C_8H_{10}Cl_2Na_2O_8$; MW = 351 g.mol^{-1}): Calc. (Found); C: 27.4 % (27.4 %); H: 2.9 % (2.8 %); Cl: 20,0 % (20.2 %); Na: 13.1 % (13.0 %); O: 36.6 % (36.6 %). Infra-red spectrum presents the characteristic peak of protonated carboxylate function[22] (1405 cm^{-1}) (Figure S5). Liquid state UV-visible absorption spectrum of a diluted aqueous solution of $Na_2(dcpa) \cdot 4H_2O$ (C = 6.8 x 10^{-5} mol.L^{-1}) has been recorded (Figure S6). It shows two maxima centered at 282 nm and 292 nm respectively. Molar absorption

coefficients have been calculated at both wavelengths: $\varepsilon_{282nm} = 680$ cm^{-1}.mol^{-1}.L and $\varepsilon_{292nm} = 560$ cm^{-1}.mol^{-1}.L.

Synthesis and characterization of the microcrystalline powders of the lanthanide based coordination polymers

Lanthanide oxides (4N) have been purchased from AMPERE and used without further purification. Chloride salts have been prepared according to established procedures.[23] Aqueous solutions of a lanthanide chloride (0.5 mmol in 20 mL) in one hand and of the sodium salt of 4,5-dichlorophthalic acid (0.75 mmol in 20 mL) in the other hand were mixed at room temperature and maintained under stirring for three days. Precipitation progressively occurred. Precipitate was filtered, washed with water and dried at ambient air. Yield was about 90 %. On the basis of their powder X-ray diffraction data, the coordination polymers were classified in two families of isostructural compounds. (i) First series is constituted by coordination polymers based on the lightest lanthanide ions (La^{3+}-Gd^{3+} except Pm^{3+}). Despite great efforts, it has not been possible, to date, to obtain single crystals suitable for single crystal X-ray diffraction. Therefore crystal structure of these compounds is still unknown. (ii) Second series gathers coordination polymers based on the heaviest lanthanide ions (Tb^{3+}-Lu^{3+}) plus Y^{3+}. These compounds have been assumed to be iso-structural to [Er$_2$(dcpa)$_3$(H$_2$O)$_5$·3H$_2$O]$_\infty$ (Figure S7) whose crystal structure is described hereafter. Chemical analyses of these compounds are reported in Table S3. IR spectra of these compounds have been performed (See Figure S8 for an example). Infra-red spectra present the characteristic peak of protonated carboxylate function[22] (1421 cm^{-1}).

It has been demonstrated that, because of their similar chemical properties,[24] it is possible to substitute one lanthanide ion by another one and therefore to obtain hetero-lanthanide coordination polymers when both corresponding homo-lanthanide

5

coordination polymers present the same crystal structure.[8-9, 15] Some hetero-lanthanide coordination polymers have been prepared in the frame of this study. Their synthesis is the same than the one described for homo-lanthanide compounds. The only difference is that the aqueous lanthanide chloride solution is replaced by an aqueous solution of the appropriate mixture of lanthanide chlorides. Relative ratio between the different lanthanide ions have been estimated by SEM measurements (See Table S4).

Synthesis of single crystals of $[Er_2(dcpa)_3(H_2O)_5 \cdot 3H_2O]_\infty$

Tetramethylorthosilicate (TMOS) was purchased from Acros Organics and used without further purification. It was jellified according to established procedures.[25-27] Dilute aqueous solutions of erbium chloride (1/4 mmol in 10 mL) in one hand and of $Na_2(dcpa) \cdot 4H_2O$ (1/4 mmol in 10 mL) in the other hand were allowed to diffuse slowly through a TMOS gel medium (7.5 % in weight) in a U-shaped tube. Needle-like single crystals suitable for X-ray structure determination appeared after few weeks (Figure 1).
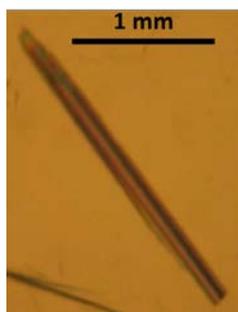
Figure 1. Picture of a needle-like single crystal of $[Er_2(dcpa)_3(H_2O)_5 \cdot 3H_2O]_\infty$.

Single crystal X-ray diffraction

Single crystal of $H_2(dcpa)$ was mounted on a Kappa CCD Bruker diffractometer and those of $Na_2(dcpa) \cdot 4H_2O$ and $[Er_2(dcpa)_3(H_2O)_5 \cdot 3H_2O]_\infty$ were mounted on an APEXII AXS-Bruker diffractometer with Mo Kα radiation (λ = 0.71073 Å). Data reductions and cell refinements were performed with Denzo and Scalepack programs.[28] The crystal structures

have been solved by direct methods using SIR97 program,[29] and refined with full matrix least-square methods based on F^2 (SHELX97[30]) with WINGX program.[31] All non-hydrogen atoms were refined anisotropically using SHELXL program. Hydrogen atoms bound to the organic ligand were located at ideal positions. Hydrogen atoms of the water molecules were not located except in the crystal structure of $Na_2(dcpa)\cdot 4H_2O$. Crystal and final structure refinement data of $[Er_2(dcpa)_3(H_2O)_5\cdot 3H_2O]_\infty$ are listed in Table 1. Full details of the X-ray structure determination of the crystal structures of $H_2(dcpa)$, $Na_2(dcpa)\cdot 4H_2O$ and $[Er_2(dcpa)_3(H_2O)_5\cdot 3H_2O]_\infty$ have been deposited with the Cambridge Crystallographic Data Center under the depository numbers CCDC-1577921, CCDC-1577920 and CCDC-229478 respectively. They can be obtained free of charge at https://www.ccdc.cam.ac.uk/structures/ [or from the Cambridge Crystallographic Data Centre, 12, Union Road, Cambridge CB2 IEZ, UK; fax: (internat.) +44-1223/336-033; E-mail: deposit@ccdc.cam.ac.uk], on request, from the authors and the reference to this publication.

Table 1. Crystal and final structure refinement data for $[Er_2(dcpa)_3(H_2O)_5\cdot 3H_2O]_\infty$	
Molecular formula	$C_{24}H_{22}Cl_6Er_2O_{20}$
System	Monoclinic
a (Å)	5.9165(1)
b (Å)	18.2813(2)
c (Å)	30.8378(5)
β (°)	91.4100(4)
V (Å^3)	3334.45(9)
Z	4
Formula weight (g.mol^{-1})	1177.64
Space group (No.)	$P2_1/n$ (14)
D_{calc} (g.cm^{-3})	2.314
μ (mm^{-1})	5.566
R (%)	7.92
R_W (%)	19.95
GoF	1.267
N° CCDC	229478

Powder X-ray diffraction

Experimental diagrams have been collected with a Panalytical X'pert Pro diffractometer equipped with an X'Celerator detector. Thermal dependent X-ray diffraction diagrams (TDXD) have been collected (between room temperature and 1000 °C under nitrogen atmosphere) with the same diffractometer equipped with an Anton Parr HTK 1200 furnace. Simulated patterns from crystal structures were produced with POWDERCELL and WINPLOTR software programs.[32-33] Pattern indexing was performed by the programs McMaille[34] and Checkcell.[35]

Optical measurements

Solid state emission and excitation spectra have been measured on a Horiba Jobin-Yvon Fluorolog III fluorescence spectrometer equipped with a Xe lamp 450 W, a UV-Vis photomultiplier (Hamamatsu R928, sensitivity 190-860 nm) and an infrared-photodiode cooled by nitrogen liquid (InGaAs, sensitivity 800-1600 nm). Most of the luminescence spectra were recorded at room temperature. Quantum yield measurements were performed using a Jobin-Yvon integrating sphere ($\Phi = (E_c\text{-}E_a)/(L_a\text{-}L_c)$ with E_c being the integrated emission spectrum of the sample, E_a the integrated "blank" emission spectrum, L_a the "blank" absorption and L_c the sample absorption at the excitation wavelength). The emission/excitation spectra and quantum yield recordings were realized on powder samples introduced in cylindrical quartz cells of 0.7 cm diameter and 2.4 cm height, which were placed directly inside the integrating sphere. The infrared emissions were measured directly on powder samples introduced in quartz capillary tubes. The phospho-luminescence of the Y-based microcrystalline powder has been measured at 77 K. The sample was introduced in a quartz capillary tube, which was placed inside a small Dewar that contained liquid nitrogen. Luminescence decays have also been measured at room temperature using this apparatus with

a Xe flash lamp (phosphorescence mode). Lifetimes and quantum yields are averages of three independent determinations.

Comparative solid state luminescent spectra have been measured on the same Horiba Jobin-Yvon Fluorolog III fluorescence spectrometer on powders samples shaped into pellets. Spectra were recorded between 450 and 725 nm under identical operating conditions and without turning the lamp off to ensure a valid comparison between the emission spectra.

Appropriate filters were used to remove the residual excitation laser light, the Rayleigh scattered light and associated harmonics from spectra. All spectra were corrected for the instrumental response function.

Luminescence intensities of the samples expressed in $Cd.m^{-2}$ have been measured with a Gigahertz-Optik X1-1 optometer with an integration time of 200 ms on 1.5 cm^2 pellets. The intensity of the UV flux at sample location, 0.9 $mW.cm^{-2}$, has been measured with a VilberLourmat VLX-3W radiometer. $[Tb_2(bdc)_3 \cdot 4H_2O]_\infty$ where bdc^{2-} stands for terephthalate was used as a standard. Its luminance is 131 $Cd.m^{-2}$ under these operating conditions (λ_{exc} = 312 nm; flux = 0.9 $mW.cm^{-2}$).[9]

Solid and aqueous solution UV-visible absorption measurements have been performed with a Perkin Elmer Lambda 650 spectrometer equipped with a 60 mm integrated sphere.

IR spectra have been recorded using a Perkin Elmer Frontier FT-IR spectrometer equipped with a UATR (Universal Attenuated Total Reflectance) accessory. Spectra have been recorded between 650 cm^{-1} and 4000 cm^{-1}, on pure samples.

Colorimetric measurements

The CIE (Commission Internationale de l'Eclairage) (x, y) emission color coordinates[36-37] were obtained using a MSU-003 colorimeter (Majantys) with the PhotonProbe 1.6.0 Software (Majantys). Color measurements: 2°, CIE 1931, step 5 nm, under

312 nm UV light. $X = k \times \int_{380nm}^{780nm} I_\lambda \times x_\lambda$, $Y = k \times \int_{380nm}^{780nm} I_\lambda \times y_\lambda$ and $Z = k \times \int_{380nm}^{780nm} I_\lambda \times z_\lambda$ with k constant for the measurement system I_λ sample spectrum intensity, wavelength depending, x_λ, y_λ, z_λ trichromatic values $x = X/(X+Y+Z)$, $y = Y/(X+Y+Z)$ and $z = Z/(X+Y+Z)$. Mean xyz values are given for each sample, which act as light sources (luminescent samples). Standards from Phosphor Technology used, calibrated at 312 nm: red phosphor $Gd_2O_2S:Eu$ ($x = 0.667$, $y = 0.330$) and green phosphor $Gd_2O_2S:Tb$ ($x = 0.328$, $y = 0.537$).

Thermal analyses

Thermal analyses (TGA/DSC) have been performed using a STA6000 Perkin Elmer thermal analyzer. The sample has been analyzed between 30 °C and 970 °C with a 20 °C/min heating rate, under di-nitrogen atmosphere (100 mL.min^{-1}) in ceramic crucibles.

Computational Details

Density functional theory (DFT) calculations were carried out using the Gaussian 09 program.[38-39] The ωB97XD[40] functional and 6-311+G* atomic basis set were employed. The three different (dcpa)$^{2-}$ structural arrangements (hereafter referenced as dcpa$_1$, dcpa$_2$ and dcpa$_3$ respectively) can be extracted from the crystal structure of $[Er_2(dcpa)_3(H_2O)_5 \cdot 3H_2O]_\infty$ obtained from X-Ray diffraction techniques. They can be mainly differentiated by the dihedral angles formed by the phenyl ring average plane and the two carboxylate planes (Schemes 2 and 3). Missing hydrogen atoms were added to the phenyl ring and their positions were optimized keeping frozen the rest of the atomic positions. These constraints allow to mimic the metal coordination and crystal packing constraints onto the (dcpa)$^{2-}$ optical properties when comparing to the free (dcpa)$^{2-}$ molecule. Indeed, their geometries were optimized to obtain a reference free geometry. The three geometry optimizations converged to

the same arrangement hereafter symbolized as dcpa$_{FREE}$. Harmonic vibrational frequency calculations were performed for dcpa$_{FREE}$ to confirm that the optimized structural arrangement corresponds to a stationary point on the potential energy surface. The Cartesian coordinates and relative energies of dcpa$_{FREE}$, dcpa$_1$, dcpa$_2$, and dcpa$_3$ are given in Table S5. Time-dependent DFT (TD-DFT) calculations were performed to compute vertical transition energies allowing access to the energies of the first singlet and triplet excited states.

RESULTS AND DISCUSSION

Reactions in water of one of the heaviest lanthanide ion (Tb^{3+}-Lu^{3+}) or Y^{3+} with the sodium salt of 4,5-dichlorophthalic acid (Na$_2$dcpa·4H$_2$O) lead to a series of isostructural compounds (Figure S7) with general chemical formula [Ln$_2$(dcpa)$_3$(H$_2$O)$_5$·3H$_2$O]$_\infty$ where Ln = Tb-Lu or Y. Crystal structure has been solved on the basis of the Er-based compound. Iso-structurality of the other compounds has been assumed on the basis of their powder X-ray diffraction diagrams (Figure S7). [Er$_2$(dcpa)$_3$(H$_2$O)$_5$·3H$_2$O]$_\infty$ can be described as a juxtaposition of molecular planes decorated by Cl atoms (Figure 2).
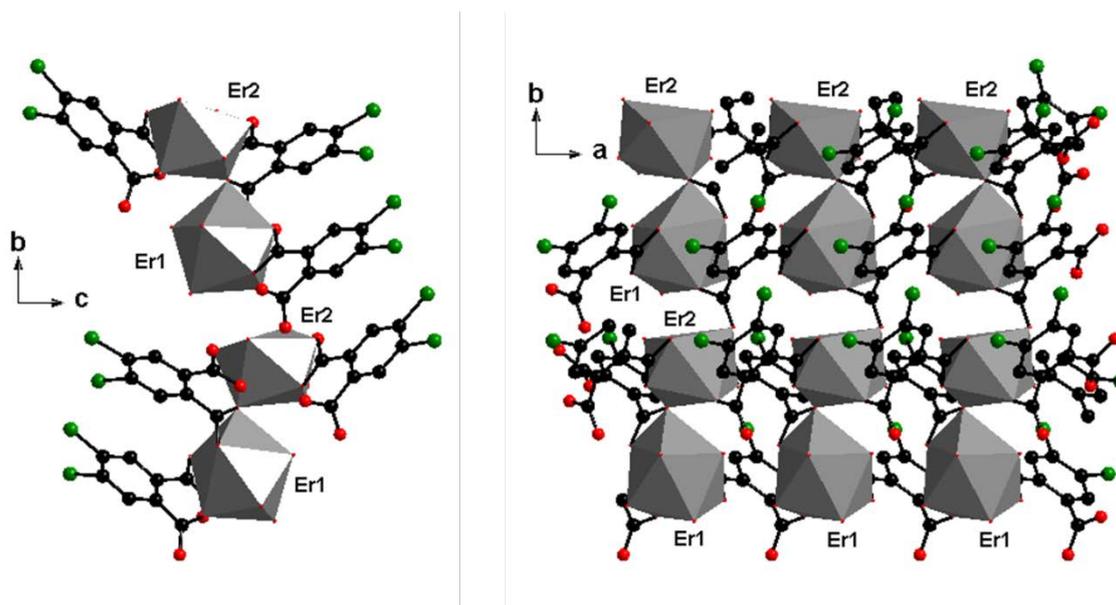
Figure 2. Projection views along the *a* (left) and *c* (right) axes of [Er$_2$(dcpa)$_3$(H$_2$O)$_5$·3H$_2$O]$_\infty$. Er polyhedra are drawn. Crystallization water molecules are omitted for clarity.

These planes that spread parallel to the (*a*,*b*) plane can be described as an alternation of two types of inorganic chains that spread along the *a* axis: First inorganic chain involves only Er1 atoms while second inorganic chain involves only Er2 atoms. Er1 atoms are nine coordinated by five oxygen atoms that belong to three different carboxylate functions from three different (dcpa)$^{2-}$ ligands and four oxygen atoms from coordination water molecules that form a slightly distorted tri-capped trigonal prism. Er2 is only eight coordinated by seven oxygen atoms from five carboxylate functions that belong to five different (dcpa)$^{2-}$ ligands and one oxygen atom from a coordination water molecule that form a slightly distorted dodecahedron. (dcpa)$^{2-}$ ligands adopt three different coordination modes as seen in Scheme 2.
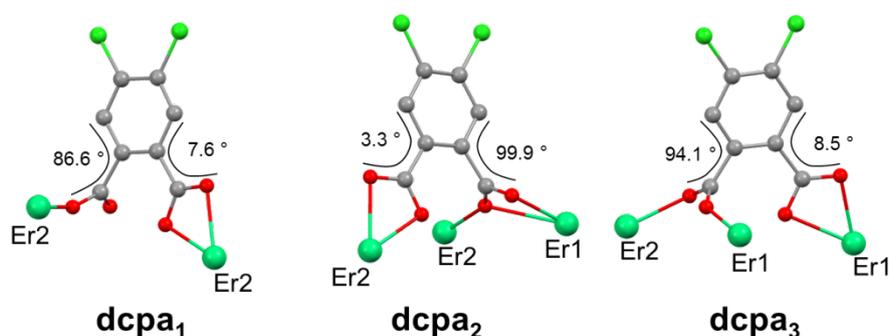
Scheme 2. Coordination modes of the ligand (dcpa)$^{2-}$. Calculated dihedral angles between the phenyl ring and the carboxylate groups are indicated.
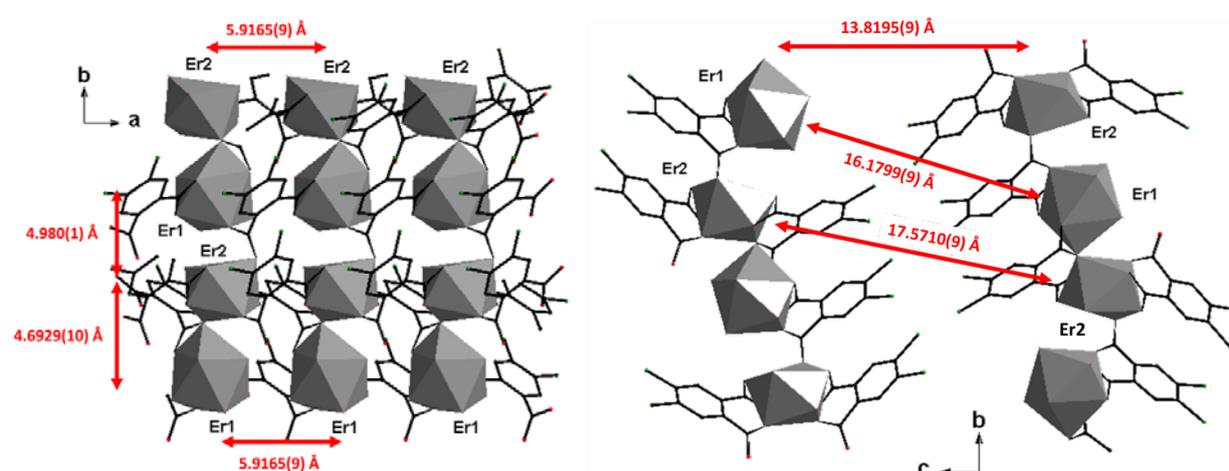

Figure 3. Intermetallic distances between lanthanide ions that belong to the same molecular plane (left) or to adjacent planes (right) in [Er$_2$(dcpa)$_3$(H$_2$O)$_5$·3H$_2$O]$_\infty$.

Lanthanide ions that belong to the same molecular plane are very close from each other (between 4.7 Å and 6 Å) (Figure 3). On the contrary, shortest intermetallic distances between lanthanide ions that belong to adjacent molecular planes are higher than 13 Å (Figure 3). Because of these uncommonly large inter-planes distances, intermetallic energy transfers between lanthanides ions that belong to different molecular planes are expected to be weak while those between lanthanide ions that belong to the same molecular plane must be efficient.[41-43] Stability of the crystal packing is insured by: hydrogen bonds, that involve crystallization and coordination water molecules; π-π interactions between adjacent phenyl rings; halogen bonds that induce the quite large space between molecular planes ($d_{Cl\text{-}Cl} \simeq 4$ Å)[44-45] (Figure 4).
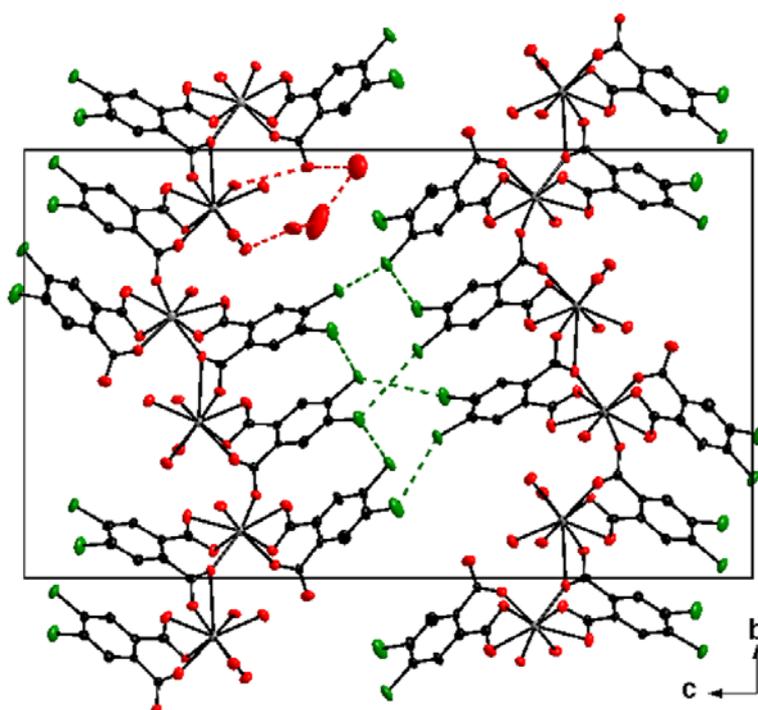
Figure 4. Projection view of an extended unit cell of $[Er_2(dcpa)_3(H_2O)_5 \cdot 3H_2O]_\infty$. Hydrogen bonds and halogen bonds are symbolized by red and green broken lines respectively.

A careful analysis of the three independent ligands geometries indicates that they are quite similar. Indeed in the three cases dihedral angles between the phenyl ring and the two carboxylate groups are very different (Schemes 2 and 3). In the three arrangements, dihedral angles for the bidentate carboxylate functions are 7.6°, 3.3° and 8.5°, for $dcpa_1$, $dcpa_2$ and

dcpa$_3$ while respectively for monodentate and bridging carboxylates functions, they are 86.6°, 99.9° and 94.1° respectively. Therefore, they show important geometrical differences compared to the free molecule dcpa$_{FREE}$ obtained by DFT calculations (see computational details). For the latter, the two dihedral angles formed by the phenyl ring average plane and the two carboxylate planes are both equal to 50.2 °. These differences clearly indicate that, despite quite weak intermolecular bounds, constraints applied by the crystal packing onto the ligand imply important rotations of the carboxylate groups.
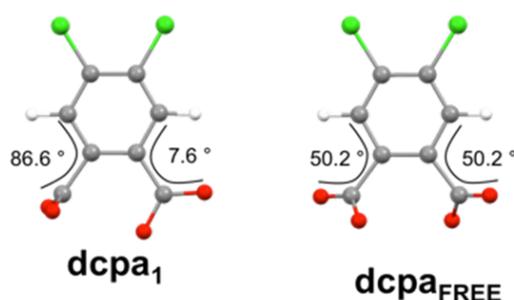
Scheme 3. Left: Geometrical arrangement of dcpa$_1$ extracted from the solid state structure of [Er$_2$(dcpa)$_3$(H$_2$O)$_5$·3H$_2$O]$_\infty$. Right: DFT fully-optimized arrangement dcpa$_{FREE}$. Calculated dihedral angles between the phenyl ring and the carboxylate groups are indicated.

Thermal behavior

Coupled TGA and DSC analyses of [Er$_2$(dcpa)$_3$(H$_2$O)$_5$·3H$_2$O]$_\infty$ have been performed (Figure 5). They show first a double endothermic weight loss between room temperature and 150 °C that can be attributed to the departure the three coordination water molecules for the first one and the five coordination water molecules for the second one. Then the resulting dehydrated phase remains stable up to 400 °C. This was confirmed by temperature dependent X-ray powder diffraction (Figure S9). The dehydrated phase is crystalline but, up to now, we did not succeed in characterizing its crystal structure. When exposed to wet atmosphere, anhydrous compound does not rehydrate. Above 400 °C, decomposition of the ligand (dcpa)$^{2-}$ occurs and leads finally to erbium oxide.
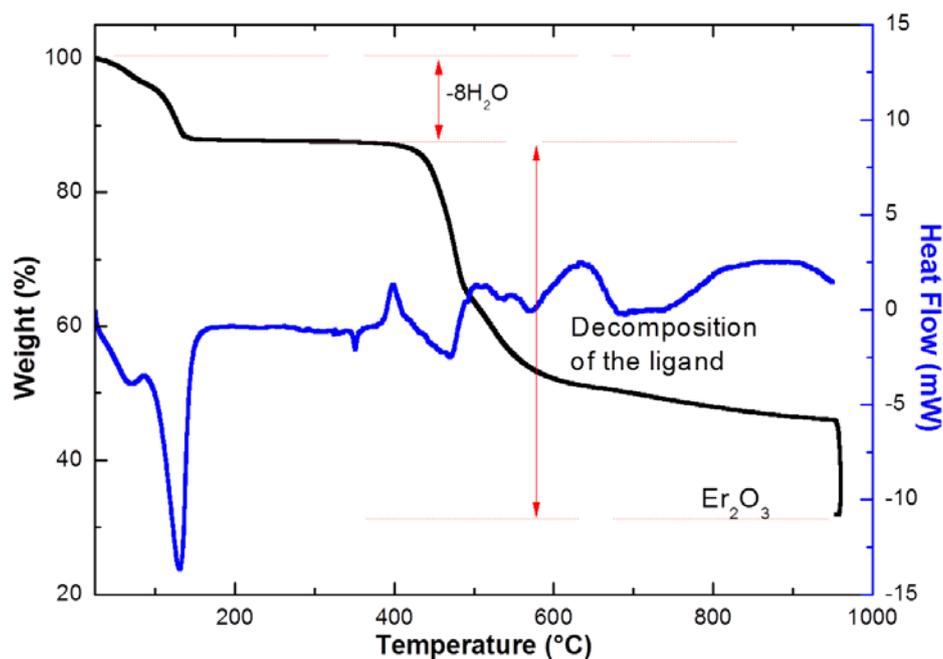
Figure 5. TGA/DSC of $[Er_2(dcpa)_3(H_2O)_5 \cdot 3H_2O]_\infty$ between room temperature and 950 °C under nitrogen atmosphere. At 950 °C, nitrogen is replaced by air in order to insure complete decomposition.

Solid state luminescence of $[Ln_2(dcpa)_3(H_2O)_5 \cdot 3H_2O]_\infty$ with Ln = Tb, Dy, Ho or Er

Solid state excitation and luminescence spectra of $[Ln_2(dcpa)_3(H_2O)_5 \cdot 3H_2O]_\infty$ with Ln = Tb, Dy, Ho or Er have been recorded (Figure 6). Excitation spectra for Tb(III) and Dy(III) show a broad band with a maximum at 302 nm which demonstrates that the ligand present an efficient "antenna effect"[46] toward these lanthanide ions. Energy levels of the first excited singlet and triplet states have been estimated by referring respectively to the UV-vis absorption edge (315 nm $\simeq$ 31750 cm^{-1}) and to the shortest wavelength of the phosphorescence band (400 nm $\simeq$ 25000 cm^{-1}) of $[Y_2(dcpa)_3(H_2O)_5 \cdot 3H_2O]_\infty$[43, 47-49] (Figures S10 and S11). Therefore, the gap between the energy levels of the first singlet and triplet excited states is $\Delta E(^1\pi* \rightarrow {}^3\pi*) \simeq 6750$ cm^{-1}. This is in agreement with Latva's[50] and Reinhoud's[51] empirical rules that state that intersystem crossing is efficient when the gap between these two energy level is higher than 5000 cm^{-1}. It is also noticeable that the

observed phosphorescence lifetime of $[Y_2(dcpa)_3(H_2O)_5 \cdot 3H_2O]_\infty$ is very long ($\tau_{obs} = 59(1)$ ms) compared with other lanthanide-based coordination polymers.[9, 11]

TD-DFT calculations have been performed in order to estimate the energy of the first singlet and triplet excited states for each of the three ligand arrangements encountered in the crystal structure (Table 2). Oscillator strengths of the singlet excited states have been calculated. In absence of spin-orbit coupling in the calculation, oscillator strengths associated to the triplet excited states are equal to zero since they are spin-forbidden. These calculations indicate that absorption of the first singlet excited states are very low for the crystal arrangements $dcpa_1$, $dcpa_2$ and $dcpa_3$ (oscillator strengths are about 10^{-3}). This is not the case for the $dcpa_{FREE}$ arrangement. Interestingly, the second singlet excited states of $dcpa_1$, $dcpa_2$ and $dcpa_3$ which lies much higher in energy than the first ones (energy differences between first and second singlet excited states are comprised between 3750 cm^{-1} and 4100 cm^{-1}), shows much higher oscillator strengths. Those are directly related to the absorbance.

Table 2. TD-DFT vertical transition energies in nm and oscillator strength of the seven first singlet excited states and two first triplet excited states of the three different arrangements of dcpa^{2-} ligands encountered in [Er$_2$(dcpa)$_3$(H$_2$O)$_5 \cdot$3H$_2$O]$_\infty$ crystal structure i. e. dcpa$_1$, dcpa$_2$, dcpa$_3$ (see Scheme 2).

	Singlet excited states (nm ; cm^{-1}) (oscillator strength)	Triplet excited states (nm ; cm^{-1})
dcpa$_1$ Dihedral angles : 7.6° / 86.6°	S$_1$: 366 ; 27322 (0.001) S$_2$: 318 ; 31446 (0.016) S$_3$: 295 ; 33898 (0.000) S$_4$: 289 ; 34602 (0.009) S$_5$: 287 ; 34843 (0.001) S$_6$: 281 ; 35587 (0.005) S$_7$: 279 ; 35842 (0.047)	T$_1$: 391 ; 25575 T$_2$: 366 ; 27322
dcpa$_2$ Dihedral angles : 3.3° / 99.9°	S$_1$: 390 ; 25575 (0.000) S$_2$: 341 ; 29325 (0.016) S$_3$: 304 ; 32895 (0.048) S$_4$: 299 ; 33333(0.000) S$_5$: 298 ; 33445 (0.008) S$_6$: 296 ; 33670 (0.011) S$_7$: 293 ; 34130 (0.001)	T$_1$: 416 ; 24038 T$_2$: 389 ; 25707
dcpa$_3$ Dihedral angles : 8.5° / 94.1°	S$_1$: 381 ; 26110 (0.001) S$_2$: 335 ; 29851 (0.009) S$_3$: 297 ; 33670 (0.016) S$_4$: 295 ; 33898 (0.005) S$_5$: 293 ; 34130 (0.000) S$_6$: 291 ; 34364 (0.031) S$_7$: 288 ; 34602 (0.010)	T$_1$: 407 ; 24570 T$_2$: 373 ; 26809

This suggests that intersystem crossing occurs between the second singlet excited states and the first triplet excited states that are separated by about 5400-5800 cm^{-1} (Scheme 4). This mechanism does not follow the usual empirical Kasha's rule.[52] However, recent improvements of time-resolved spectroscopies have revealed much more complex optical de-excitation schemes in lot of cases where higher excited states than the first singlet and triplet excited states are involved.[53-54]
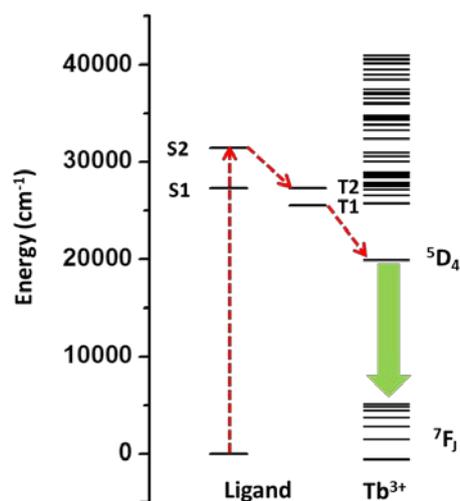
Scheme 4 . Schematic Jablonski diagram of the different energy transfers.

This assumption is also supported by the energies of the second singlet excited states that range between 318 nm and 341 nm and by the energies of the first triplet excited states that range between 391 nm and 416 nm which is in good agreement with experimental values.

Figure 6. Solid state excitation and emission spectra of $[Ln_2(dcpa)_3(H_2O)_5 \cdot 3H_2O]_\infty$ with Ln = Tb(III), Dy(III), Ho(III) or Er(III) (from top to bottom) at 77 K or 293 K.
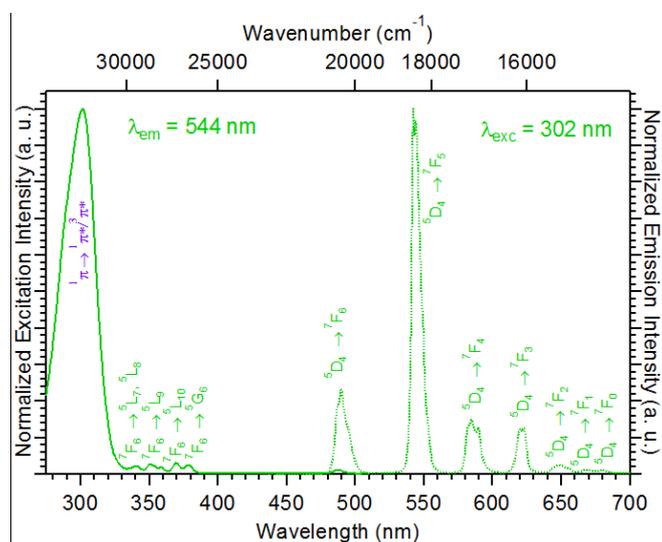
Excitation spectrum of the Tb-based compound (Figure 6) shows a very efficient antenna effect which is in agreement with Latva's empirical rule[50] that predicts that the energy of the lowest excited triplet state (25000 cm^{-1}) favors an efficient ligand-to-metal energy transfer without significant back-transfer. Figure 6 also shows the emission upon UV-irradiation (λ_{exc} = 302 nm) with the seven classical narrow bands from Tb(III) that are attributed to the transitions $^5F_4 \rightarrow {}^7F_6$, $^7F_5$, $^7F_4$, $^7F_3$, $^7F_2$, $^7F_1$ and $^7F_0$ centered at 490, 542.5, 585, 621.5, 648.5, 669 and 680 nm, respectively. Overall quantum yield (Q_{Tb}^{Ligand} = 32.6(2) %) and observed luminescent lifetime (τ_{obs}= 0.97(1) ms) under UV light (λ_{exc} = 302 nm) are quite large and compare well with values that were obtained in previous studies.[9, 15, 55] Despite very short intermetallic distances in the molecular motif, a sizeable luminescence intensity under UV light (λ_{exc} = 312 nm) has been measured (153(4) Cd.m^{-2} under a 0.9 mW.cm^{-2} luminous flux). To the best of our knowledge, only few coordination polymers exhibit higher luminance in similar operating conditions.[15]

Excitation spectrum of the Dy-based compound reveals a classical broad band at high energy corresponding to (dcpa)$^{2-}$ ligand, stimulating a lower antenna effect compared to the Tb-based compound. Because of its small energy gap[56] the Dy-based compound presents a much weaker luminescence under UV light (λ_{exc} = 302 nm) than the Tb-based compound. Emission spectrum shows the classical four bands from Dy(III) that are attributed to the transitions $^4F_{9/2} \rightarrow {}^6H_{15/2}$, $^6H_{13/2}$, $^6H_{11/2}$ and $^6H_{9/2}$ centered at 478.5, 573.5, 660.5 and 751 nm, respectively. A relatively low overall quantum yield (Q_{Dy}^{Ligand} = 0.16(1) %) has been measured. The observed luminescent lifetime can't be measured for the Dy(III) with our current setup because the lifetime for Dy(III) is lower to 20 µs (the limit of the flash lamp and spectrometer).

Excitation spectrum for the Ho-based compound is particularly weak compared to Tb-, Dy-based compounds and does not reveal any characteristic band from the (dcpa)$^{2-}$ ligand. Visible emission has been measured; the usual red band from Ho(III) centered at 659.5 nm is observed, attributed to the transitions $^5F_3 \rightarrow {}^5I_7$ and $^5F_5 \rightarrow {}^5I_8$. An additional band in the visible is observed at 538 nm which is assigned to the transition $^5F_4 \leftrightarrow {}^5I_8$. The particularity of the transition is that it is observed by a dip corresponding to internal holmium-centered re-absorption of the broad residual ligand centered $^1\pi^* \rightarrow {}^1\pi$ emission (Figure S12).[57-58] An infrared band centered at 977 nm, assigned to the transitions $^5F_5 \rightarrow {}^5I_7$ and $^5F_4 \rightarrow {}^5I_6$ has also been observed.

For Er(III) compound, emission spectrum reveals a low transition with a maximum at 557 nm and a shoulder at 542 nm, that can attributed to transitions $^2H_{9/2}, {}^2G_{9/2}, {}^4F_{9/2} \rightarrow {}^4I_{13/2}$ and $^4S_{3/2} \rightarrow {}^4I_{15/2}$ respectively, characteristic to a weak green emission of the erbium(III). At higher energy, some dips are observed as in the erbium(III) compound, all dips are characteristic from the internal erbium-centered reabsorption of the broad residual ligand centered $^1\pi^* \rightarrow {}^1\pi$ emission ($^2H_{11/2}, {}^4F_{7/2}, ({}^4F_{5/2}, {}^4F_{3/2}) \leftrightarrow {}^4I_{15/2}$ at 520, 488 and 453 nm, respectively). The characteristic infrared emission of Er(III) has been also observed at 77 K at approximately 1536 nm, showing the transition $^4I_{13/2} \rightarrow {}^4I_{15/2}$.

Hetero-lanthanide coordination polymers, $[Tb_{2-2x}Y_{2x}(dcpa)_3(H_2O)_5 \cdot 3H_2O]_\infty$ and $[Tb_{2-2x}Eu_{2x}(dcpa)_3(H_2O)_5 \cdot 3H_2O]_\infty$ with $0 \leq x \leq 1$, that exhibit emission in the visible

A series of hetero-lanthanide compounds with general chemical formula $[Tb_{2-2x}Y_{2x}(dcpa)_3(H_2O)_5 \cdot 3H_2O]_\infty$ with $0 \leq x \leq 1$ has been prepared. On the basis of their powder diffraction all the compounds of the series have been assumed to be isostructural to $[Er_2(dcpa)_3(H_2O)_5 \cdot 3H_2O]_\infty$ (Figure S13). Composition of the compounds has been estimated

on the basis of SEM measurements (Table S4). Luminescence spectra have been recorded and their integrated intensities calculated (Figure 7).
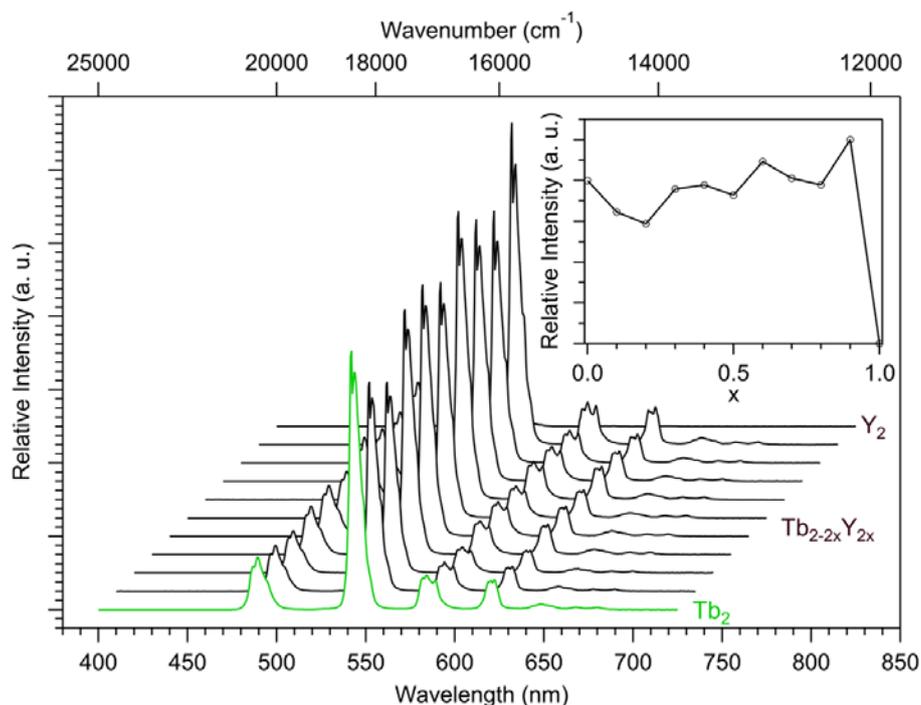

Figure 7. Emission spectra of $[Tb_{2-2x}Y_{2x}(dcpa)_3(H_2O)_5 \cdot 3H_2O]_\infty$ with $0 \leq x \leq 1$ versus x ($\lambda_{exc} = 302$ nm) at 293 K. In inset: maximum intensities versus x.

As expected these spectra clearly show that dilution of Tb^{3+} ions by optically non-active Y^{3+} ions provokes an enhancement of the luminescence of the Tb^{3+} ions. The more intense luminescence is observed for $[Tb_{0.2}Y_{1.8}(dcpa)_3(H_2O)_5 \cdot 3H_2O]_\infty$, that is $x = 0.9$. This value is in good agreement with the empirical rule that states that intermetallic energy transfers are less efficient when lanthanide ions are more than 10 Å far from each other. Indeed, this crystal structure can be described as the superimposition of molecular layers that are separated by more than 13 Å. On the opposite, in a molecular layer, each lanthanide ion is surrounded by 10 other lanthanide ions which are closer than 10 Å from it (Scheme 5). Therefore, according to this quite rough model, luminescence intensity is expected to reach a maximum for $x = 0.91$.[59]
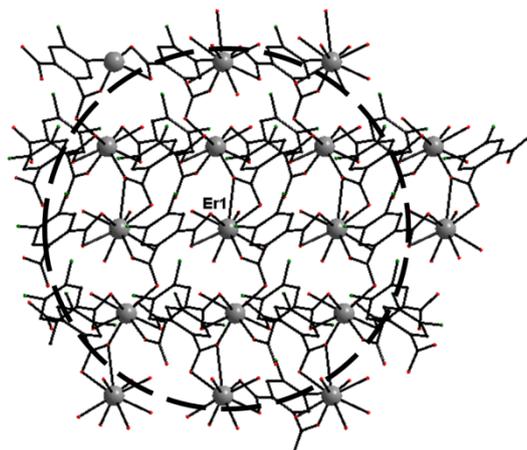
Scheme 5. Schematic representation of the neighborhood of a Er^{3+} ion in a molecular layer of $[Er_2(dcpa)_3(H_2O)_5 \cdot 3H_2O]_\infty$. The radius of the dotted circle is 10 Å.

Hetero-lanthanide compounds with general chemical formula $[Tb_{2-2x}Eu_{2x}(dcpa)_3(H_2O)_5 \cdot 3H_2O]_\infty$ with $0 \leq x \leq 1$ have also been prepared. Their composition has been estimated on the basis of SEM measurements (Table S4). Powder X-ray diffraction diagrams show that compounds with $x \leq 0.5$ are isostructural to $[Er_2(dcpa)_3(H_2O)_5 \cdot 3H_2O]_\infty$ (Figure S14) while those with $x \geq 0.6$ are isostructural to the lightest lanthanide-based compounds.

In the following, we have focused our attention on compounds with $x \leq 0.5$ because of its isostructurality with the reported crystal structure. Because intermetallic distances between lanthanide ions that belong to the same molecular plane are short, intermetallic energy transfers are expected to be efficient and therefore it must be possible to observe a sizeable Tb^{3+}-to-Eu^{3+} intermetallic energy transfer. Accordingly this may provide access to red luminescence in this family of compounds despite the fact that the Eu-based compound does not belong to the series of compounds isostructural to $[Er_2(dcpa)_3(H_2O)_5 \cdot 3H_2O]_\infty$. Indeed, excitation spectra (Figure 8) show that the characteristic peak of Tb^{3+} centered at 542 nm ($^5D_4 \rightarrow {}^7F_5$) abruptly decreases and almost disappears as soon as x becomes greater than 0.2. At the same time, the characteristic peak of Eu^{3+} centered at 615 nm ($^5D_0 \rightarrow {}^7F_2$) increases and

reaches a maximum at $x = 0.1$ and then decreases slowly although Eu^{3+} contents increases. This suggests that feeding of the luminescent levels of the Eu^{3+} ions is more efficient via a two steps Ligand-to-Tb^{3+}-to-Eu^{3+} energy transfer than from direct Ligand-to Eu^{3+} one. This was unexpected and to the best of our knowledge never reported before.
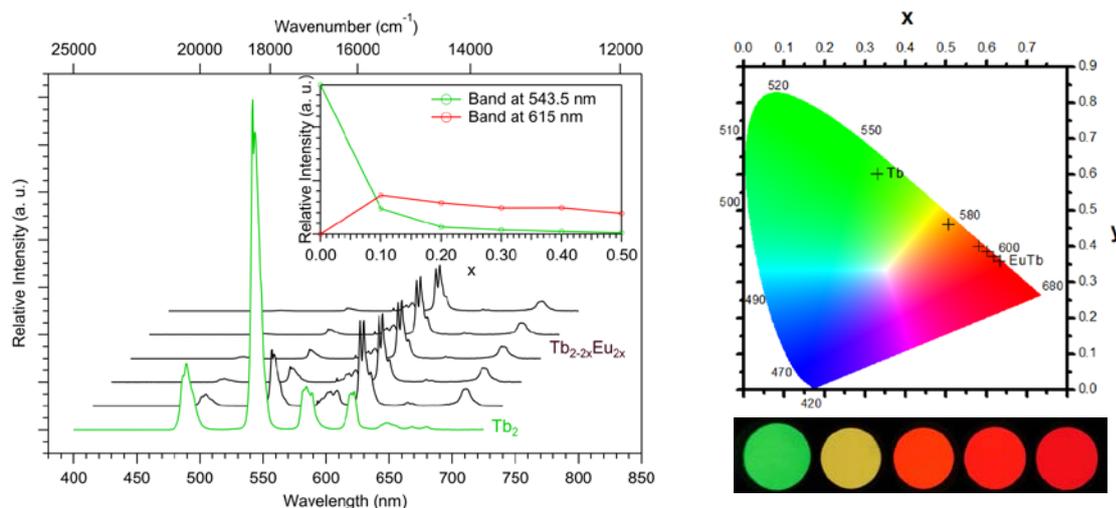

Figure 8. Left : Luminescence spectra of $[Tb_{2-2x}Eu_{2x}(dcpa)_3(H_2O)_5 \cdot 3H_2O]_\infty$ with $0 \leq x \leq 0.5$ versus x ($\lambda_{exc} = 302$ nm) at 293 K. In inset, integrated intensities of the major characteristic emission peaks of Tb^{3+} and Eu^{3+} centered at 543.5 nm ($^5D_4 \rightarrow {^7F_5}$) and 615 nm ($^5D_0 \rightarrow {^7F_2}$) respectively. Right : Colorimetric coordinates ($\lambda_{exc} = 302$ nm) (top) and pictures ($\lambda_{exc} = 312$ nm) (bottom) of $[Tb_{2-2x}Eu_{2x}(dcpa)_3(H_2O)_5 \cdot 3H_2O]_\infty$ with $0 \leq x \leq 0.5$ under UV irradiation at 293 K.

Terbium-to Europium energy transfer efficiency (η_{ET}) can be estimated by using the relationship:

$$\eta_{ET} = 1 - \frac{\tau_{obs}}{\tau_0} \tag{1}$$

where τ_{obs} and τ_0 are the luminescent lifetimes measured in presence and in absence of an acceptor ion.[56] Therefore excitation and emission spectra of $[Tb_{1.6}Eu_{0.4}(dcpa)_3(H_2O)_5 \cdot 3H_2O]_\infty$ and $[Tb_{1.6}Y_{0.4}(dcpa)_3(H_2O)_5 \cdot 3H_2O]_\infty$ (Figures S15 and S16, respectively) have been recorded and their overall quantum yields ($Q_{Ln^{3+}}^{Ligand}$) and luminescent lifetimes measured. They are listed in Table 3. Additionally excitation and emission spectra of

24

$[Y_{1.6}Eu_{0.4}(dcpa)_3(H_2O)_5\cdot 3H_2O]_\infty$, which is isostructural to $[Er_2(dcpa)_3(H_2O)_5\cdot 3H_2O]_\infty$ (Figure S17 and Table S4), have also been recorded (Figure S18) and overall quantum yield and luminescent lifetimes measured (Table 3).

Table 3. Overall quantum yields and luminescent lifetimes for $[Ln_{1.6}Ln'_{0.4}(dcpa)_3(H_2O)_5\cdot 3H_2O]_\infty$ with Ln = Tb or Y and Ln' = Eu or Y.

	Tb^{3+}		Eu^{3+}	
	$Q^{Ligand}_{Tb^{3+}}$ (%)	τ_{obs} (ms)	$Q^{Ligand}_{Eu^{3+}}$ (%)	τ_{obs} (ms)
$[Tb_{1.6}Eu_{0.4}(dcpa)_3(H_2O)_5\cdot 3H_2O]_\infty$	3.0(1)	0.21(1)	14.9(1)	0.43(1)
$[Tb_{1.6}Y_{0.4}(dcpa)_3(H_2O)_5\cdot 3H_2O]_\infty$	81(1)	0.92(1)	-	-
$[Y_{1.6}Eu_{0.4}(dcpa)_3(H_2O)_5\cdot 3H_2O]_\infty$	-	-	15.0(1)	0.58(1)

This table clearly shows that the Tb^{3+}-to-Eu^{3+} intermetallic energy transfer is particularly efficient in these compounds: $Q^{Ligand}_{Tb^{3+}}$ decreases from approximately 80 % to 3 % when Y^{3+} is replaced by Eu^{3+} and $Q^{Ligand}_{Eu^{3+}}$ stays stable around 15% when Y^{3+} is replaced by Tb^{3+}. Terbium-to Europium energy transfer efficiency (η_{ET}) can be estimated to 77 % according to relationship (1). This high value makes the feeding of the luminescent energy level of Eu^{3+} ions as efficient via Tb^{3+} to Eu^{3+} intermetallic energy transfer as by direct Ligand-to-Eu^{3+} "antenna effect". Unfortunately, it has not been possible to evaluate intrinsic quantum yields for Tb^{3+} ions nor for Eu^{3+} ions. This can probably be related to the first single excited states that overlap with 4f-4f absorption bands centered at 379 nm for Tb^{3+} and 395 nm for Eu^{3+}. Indeed even if absorption bands of the ligand are weak they are stronger than the forbidden 4f-4f transitions.

Hetero-lanthanide coordination polymer $[Y_{1.8}Nd_{0.2}(dcpa)_3(H_2O)_5\cdot 3H_2O]_\infty$ with emission in the IR

These results show that light lanthanide can be incorporated to this system provided their doping rates remain reasonably low. In order to test the IR emitting capability of this

system, $[Y_{1.8}Nd_{0.2}(dcpa)_3(H_2O)_5 \cdot 3H_2O]_\infty$ has been prepared. Because of its high Y^{3+} content, this compound is iso-structural to $[Er_2(dcpa)_3(H_2O)_5 \cdot 3H_2O]_\infty$ (Figure S19 and Table S4). Its excitation and emission spectra have been recorded (Figure 9) at room temperature.
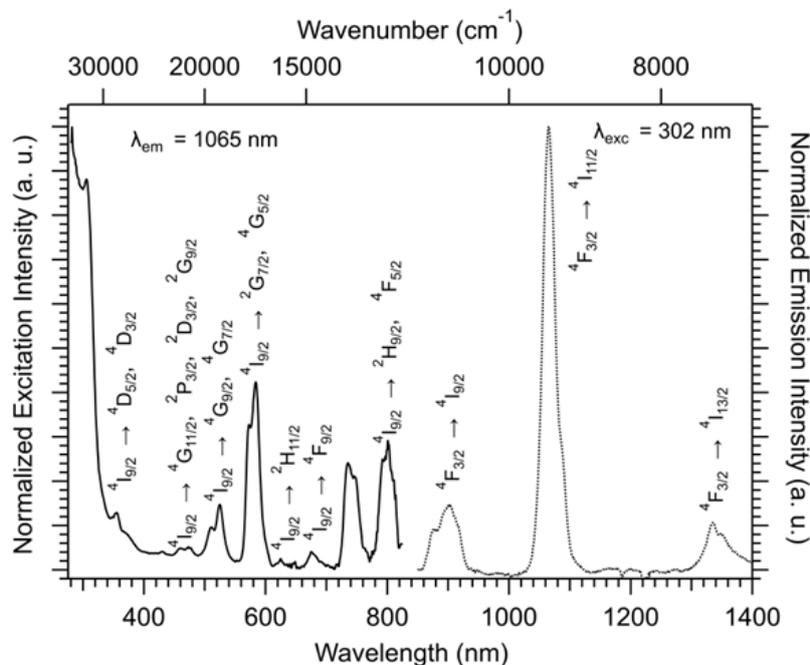

Figure 9. Excitation and emission spectra of $[Y_{1.8}Nd_{0.2}(dcpa)_3(H_2O)_5 \cdot 3H_2O]_\infty$ at 293 K.

Excitation spectrum indicates that $dcpa^{2-}$ has an efficient "antenna effect" toward Nd^{3+} ion. Emission spectrum shows the classical emission bands from Nd(III) that are attributed to the transitions $^4F_{3/2} \rightarrow {}^4I_{9/2}$, $^4I_{11/2}$ and $^4I_{13/2}$ centered at 900, 1065 and 1334 nm, respectively. The excitation spectrum shows some thin bands between 350 and 825 nm corresponding to the f-f transitions for Nd(III) as shown in Figure 9. This sizeable emission in the IR region is particularly interesting as far as multi-emission luminescent materials are targeted. Indeed, it opens the way to hetero-poly-lanthanide coordination polymers that would emit in both the visible and the IR domains under a unique UV irradiation. Because of their potential technical applications in the field of luminescent barcodes, multi-emissive coordination compounds have aroused great interest in recent years and several interesting compounds have been reported.[17, 60-63] However, emission modulation was either induced by varying excitation

wavelength or emission was restricted to a sharp emission wavelength range. To the best of our knowledge, examples of coordination compounds that can simultaneously (that is, under the same excitation radiation) emit both in IR and visible regions are scarce.

Hetero-lanthanide coordination polymers $[Y_{0.4}Tb_{1.26}Eu_{0.14}Nd_{0.2}(dcpa)_3(H_2O)_5 \cdot 3H_2O]_\infty$ with dual emission in the visible and IR regions

We have prepared the compound $[Y_{0.4}Tb_{1.26}Eu_{0.14}Nd_{0.2}(dcpa)_3(H_2O)_5 \cdot 3H_2O]_\infty$ in which Y^{3+} ions are expected not only to act as non-active optical spacers but also to impose the crystal structure. As expected, this compound is iso-structural to $[Er_2(dcpa)_3(H_2O)_5 \cdot 3H_2O]_\infty$ (Figure S20 and Table S4). Its excitation and luminescence spectra have been recorded (Figures 10, S21 and S22).
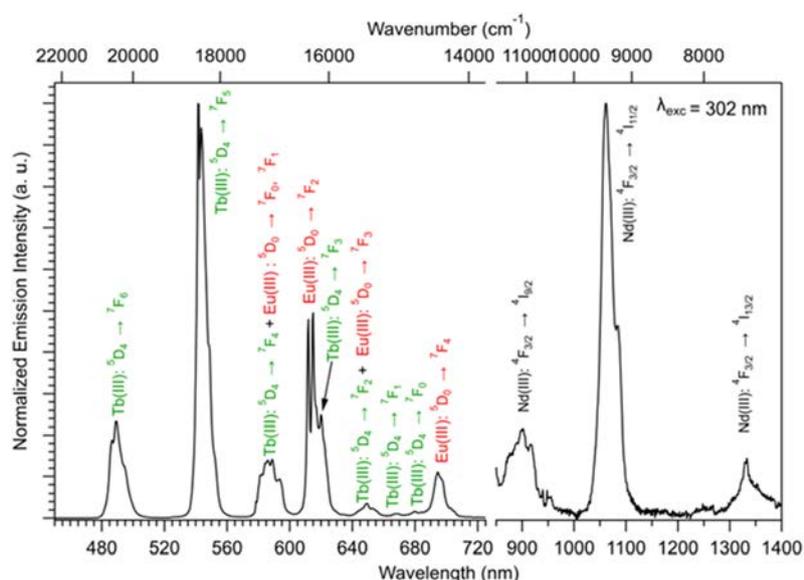

Figure 10. Visible and Infra-Red emission spectrum of $[Y_{0.4}Tb_{1.26}Eu_{0.14}Nd_{0.2}(dcpa)_3(H_2O)_5 \cdot 3H_2O]_\infty$ at 293 K. $\lambda_{exc} = 302$ nm.

These spectra (S21 and S22) confirm that dcpa^{2-} ligand can act as an efficient "antenna effect" toward Eu^{3+}, Tb^{3+} and Nd^{3+}. Emission spectrum presents the characteristic peaks of the three optically active lanthanide ion, that is 615 nm for Eu^{3+}, 542 nm for Tb^{3+} and 1062 nm for Nd^{3+}, with sizeable intensities. This validates the fact that some compounds of this series

can be interesting as far as luminescent barcodes stretching over a large emission wavelength range are targeted.

CONCLUSIONS AND OUTLOOKS

A new series of iso-structural lanthanide coordination polymers has been synthesized. Homo-lanthanide coordination polymers that belong to this family have general chemical formula $[Ln_2(dcpa)_3(H_2O)_5 \cdot 3H_2O]_\infty$ with Ln = Tb-Lu plus Y and some of them exhibit intense luminescence. This series can be extended to hetero-lanthanide compounds by mixing two or more of these heaviest lanthanide ions as often reported previously. Originality of this series lies in two points: First it is possible to extend the family to hetero-lanthanide coordination compounds that involve some light lanthanide ions in a reasonable doping rate; second, some of the lightest lanthanide-containing compounds exhibit quite intense luminescence in the IR region as exemplified by the Nd-based compounds described above. This makes possible the design of Eu-Tb-Nd-based compounds that present efficient emission in both visible and IR regions under a unique excitation wavelength. This is of great interest as far as luminescent barcodes are targeted. This strategy also relies on the use of lanthanide ions, such as Y^{3+}, that on one hand impose the crystal structure and on the other hand prevent intermetallic quenching. An extremely wide variety of such compounds could be synthesized in the near future.

CONFLICT OF INTEREST.

The authors declare no conflict of interest.

SUPPORTING INFORMATION.

Projection view of an asymmetric unit of $H_2(dcpa)$ (Figure S1) ; Crystal and final structure refinement data for $H_2(dcpa)$ (Table S1) ; Projection view of an asymmetric unit of $Na_2(dcpa) \cdot 4H_2O$ (Figure S2) ; Crystal and final structure refinement data for $Na_2(dcpa) \cdot 4H_2O$ (Table S2) ; Experimental and simulated powder X-ray diffraction patterns of $Na_2(dcpa) \cdot 4H_2O$ (Figure S3) ; Thermal analysis (TGA/TDA) of $Na_2(dcpa) \cdot 4H_2O$ (Figure S4) ; Infra-red spectrum of $Na_2(dcpa) \cdot 4H_2O$ (Figure S5) ; Liquid state UV-visible absorption spectrum of a dilute aqueous solution of $Na_2(dcpa) \cdot 4H_2O$ (Figure S6) ; Experimental X-ray diffraction diagrams of the lanthanide-based coordination polymers with $(dcpa)^{2-}$ as ligand (Figure S7) ; Chemical analyses of $[Ln_2(dcpa)_3(H_2O)_5 \cdot 3H_2O]_\infty$ (Table S3) ; IR spectrum of $[Tb_2(dcpa)_3(H_2O)_5 \cdot 3H_2O]_\infty$ (Figure S8) ; Relative lanthanide contents in hetero-lanthanide coordination polymers (Table S4) ; Cartesian coordinates and total energies of $dcpa_1$, $dcpa_2$, $dcpa_3$ and $dcpa_{FREE}$ (Table S5) ; TDXD measurements for $[Er_2(dcpa)_3(H_2O)_5 \cdot 3H_2O]_\infty$ (Figure S9) ; Solid state UV-visible absorption of $[Y_2(dcpa)_3(H_2O)_5 \cdot 3H_2O]_\infty$ (Figure S10) ; Solid state phosphorescence and excitation spectra of $[Y_2(dcpa)_3(H_2O)_5 \cdot 3H_2O]_\infty$ at 77 K (Figure S11) ; Solid state excitation and emission spectra of $[Ho_2(dcpa)_3(H_2O)_5 \cdot 3H_2O]_\infty$ at 77 K (Figure S12) ; Powder X-ray diffraction diagrams of $[Tb_{2-2x}Y_{2x}(dcpa)_3(H_2O)_5 \cdot 3H_2O]_\infty$ with $0 \leq x \leq 1$ (Figure S13) ; Powder X-ray diffraction diagrams of $[Tb_{2-2x}Eu_{2x}(dcpa)_3(H_2O)_5 \cdot 3H_2O]_\infty$ with $0 \leq x \leq 0.5$ (Figure S14) ; Solid state excitation and emission spectra of $[Tb_{1.6}Eu_{0.4}(dcpa)_3(H_2O)_5 \cdot 3H_2O]_\infty$ (Figure S15) ; Solid state excitation and emission spectra of $[Tb_{1.6}Y_{0.4}(dcpa)_3(H_2O)_5 \cdot 3H_2O]_\infty$ (Figure S16) ; Experimental X-ray diffraction diagrams of $[Y_{1.6}Eu_{0.4}(dcpa)_3(H_2O)_5 \cdot 3H_2O]_\infty$ and simulated pattern from the crystal structure of

$[Er_2(dcpa)_3(H_2O)_5 \cdot 3H_2O]_\infty$ (Figure S17) ; Solid state excitation and emission spectra of $[Y_{1.6}Eu_{0.4}(dcpa)_3(H_2O)_5 \cdot 3H_2O]_\infty$ (Figure S18) ; Experimental X-ray diffraction diagrams of $[Y_{1.8}Nd_{0.2}(dcpa)_3(H_2O)_5 \cdot 3H_2O]_\infty$ and simulated pattern from the crystal structure of $[Er_2(dcpa)_3(H_2O)_5 \cdot 3H_2O]_\infty$ (Figure S19) ; Experimental X-ray diffraction diagrams of $[Y_{0.4}Tb_{1.26}Eu_{0.14}Nd_{0.2}(dcpa)_3(H_2O)_5 \cdot 3H_2O]_\infty$ and simulated pattern from the crystal structure of $[Er_2(dcpa)_3(H_2O)_5 \cdot 3H_2O]_\infty$ (Figure S20) ; Solid state excitation and visible emission spectra of $[Y_{0.4}Tb_{1.26}Eu_{0.14}Nd_{0.2}(dcpa)_3(H_2O)_5 \cdot 3H_2O]_\infty$ (Figure S21) ; Solid state excitation and infrared emission spectra of $[Y_{0.4}Tb_{1.26}Eu_{0.14}Nd_{0.2}(dcpa)_3(H_2O)_5 \cdot 3H_2O]_\infty$ (Figure S22).

REFERENCES

1.   Cui, Y.; Li, B.; He, H.; Zhou, W.; Chen, B.; Qian, G., Metal-organic frameworks as platforms for functionnal materials. *Accounts Chem. Res.* **2016,** *49*, 483-493.

2.   Cui, Y.; Yue, Y.; Qian, G.; Chen, B., Luminescent Functional Metal-Organic Frameworks. *Chem. Rev.* **2012,** (111), 1126-1162.

3.   Bünzli, J. C. G., On the design of highly luminescent lanthanide complexes. *Coord. Chem. Rev.* **2015,** *293-294*, 19-47.

4.   Eliseeva, S. V.; Bünzli, J. C. G., Rare earths : jewels for functionnal materials of the future. *New J. Chem.* **2011,** *35*, 1165-1176.

5.   Bünzli, J.-C. G., Lanthanide luminescence for biomedical analyses and imaging. *Chem. Rev.* **2010,** *111*, 2729-2755.

6.   Bünzli, J. C. G., Rising stars in science and technology : Luminescent lanthanide materials. *Eur. J. Inorg. Chem.* **2017**, 5058-5063.

7.   Daiguebonne, C.; Gérault, Y.; Guillou, O.; Lecerf, A.; Boubekeur, K.; Batail, P.; Kahn, M.; Kahn, O., A new honeycomb-like molecular compound : Gd[C 6H3(COO)3](H2O)3.1.5H2O *J. Alloys Compd.* **1998,** *275-277*, 50-53.

8.   Freslon, S.; Luo, Y.; Daiguebonne, C.; Calvez, G.; Bernot, K.; Guillou, O., Brightness and color tuning in a series of lanthanide-based coordination polymers with benzene 1,2,4,5-tetracarboxylic acid as ligand. *Inorg. Chem.* **2016,** *55*, 794-802.

9.   Haquin, V.; Etienne, M.; Daiguebonne, C.; Freslon, S.; Calvez, G.; Bernot, K.; Le Polles, L.; Ashbrook, S. E.; Mitchell, M. R.; Bünzli, J. C. G.; Guillou, O., Color and Brightness tuning in hetero-nuclear laanthanide teraphthalate coordination polymers. *Eur. J. Inorg. Chem.* **2013**, 3464-3476.

10.   Le Natur, F.; Calvez, G.; Daiguebonne, C.; Guillou, O.; Bernot, K.; Ledoux, J.; Le Polles, L.; Roiland, C., Coordination polymers based on hexanuclear rare earth complexes : Toward independant luminescence brightness and color emission. *Inorg. Chem.* **2013,** *52*, 6720-6730.

11.   Kerbellec, N.; Kustaryono, D.; Haquin, V.; Etienne, M.; Daiguebonne, C.; Guillou, O., An Unprecedented Family of Lanthanide-Containing Coordination Polymers with Highly Tunable Emission Properties. *Inorg. Chem.* **2009,** *48* (7), 2837-2843.

12.   Gooch, J.; Daniel, B.; Abbate, V.; Frascione, N., Taggant materials in forensic science. *Trends Anal. Chem.* **2016,** *83*, 49-54.

13.   Guillou, O.; Daiguebonne, C.; Calvez, G.; Bernot, K., A long journey in lanthanide chemistry : from fundamental crystallogenesis studies to commercial anti-counterfeiting taggants. *Accounts Chem. Res.* **2016,** *49*, 844-856.

14.   Andres, J.; Hersch, R. D.; Moser, J. E.; Chauvin, A. S., A new counterfeiting feature relying on invisible luminescent full color images printed with lanthanide-based Inks. *Adv. Func. Mater.* **2014,** *24*, 5029-5036.

15.   Badiane, I.; Freslon, S.; Suffren, Y.; Daiguebonne, C.; Calvez, G.; Bernot, K.; Camara, M.; Guillou, O., High brightness and easy color modulation in lanthanide-based coordination polymers with 5-methoxyisophthalate as ligand: Toward emission colors additive strategy. *Cryst. Growth Des.* **2017,** *17* (3), 1224-1234.

16.   Freslon, S.; Luo, Y.; Calvez, G.; Daiguebonne, C.; Guillou, O.; Bernot, K.; Michel, V.; Fan, X., Influence of photo-induced electron transfer on lanthanide-based coordination polymers luminescence : A comparison between two pseudo-isoreticular molecular networks. *Inorg. Chem.* **2014,** *53*, 1217-1228.

17.   Fan, X.; Freslon, S.; Daiguebonne, C.; Calvez, G.; Le Polles, L.; Bernot, K.; Guillou, O., Heteronuclear lanthanide-based coordination polymers exhibiting tunable multiple emission spectra. *J. Mater. Chem. C* **2014**, 5510-5525.

18.   Luo, Y.; Calvez, G.; Freslon, S.; Bernot, K.; Daiguebonne, C.; Guillou, O., Lanthanide amino-isophthalate coordination polymers. A promising system for tunable luminescent properties. *Eur. J. Inorg. Chem.* **2011**, 3705-3716.

19.   Cui, H.-W.; Xia, Y.-F.; Xiang, X.-X.; Qin, S.-H.; Yang, E. C., Synthesis, structure and magnetism of two Cu(II) 4,5-dichlorophthalate complexes. *Chin. J. Struct. Chem.* **2015,** *34* (12), 1862-1868.

20.   Zorlu, Y.; Can, H., Self assembly of sandwich-layered 2D silver(I) coordination polymers stabilized by argentophilic interactions : synthesis, crystal structures and ab initio intramolecular energetics. *J. Mol. Struc.* **2014,** *1076*, 629-638.

21.   Shaw, S. D.; Blum, A.; Weber, R.; Kannan, K.; Rich, D.; Lucas, D.; Koshland, C. P.; Dobraca, D.; Hanson, S.; Birnbaum, L. S., Halogenated flame retardants : do the fire safety benefits justify the risks ? *Rev. Environ. Health* **2010,** *25* (4), 261-305.

22.   Varghese, H. T.; Panicker, C. Y.; Philip, D.; Sreevalsan, K.; Anithakumary, V., IR, Raman and SERS spectra of disodium therephthalate. *Spectrochimica Acta Part A* **2007,** (68), 817-822.

23.   Desreux, J. F., In *Lanthanide Probes in Life, Chemical and Earth Sciences*, Choppin, G. R.; Bünzli, J. C. G., Eds. Elsevier: Amsterdam, 1989; Vol. Elsevier, p 43.

24.   Karraker, D. G., Coordination of trivalent lanthanide ions. *J. Chem. Educ.* **1970,** *47* (6), 424-430.

25.   Henisch, H. K., *Crystals in Gels and Liesegang Rings*. Cambridge University Press: Cambridge, 1988.

26.   Henisch, H. K.; Rustum, R., *Crystal Growth in Gels*. The Pennsylvania State University Press: 1970; p 1-196.

27.   Daiguebonne, C.; Deluzet, A.; Camara, M.; Boubekeur, K.; Audebrand, N.; Gérault, Y.; Baux, C.; Guillou, O., Lanthanide-based molecular materials : gel medium induced polymorphism. *Cryst. Growth Des.* **2003,** *3* (6), 1015-1020.

28.   Minor, W.; Cymborowski, M.; Otwinowski, Z.; Chruszcz, M., HKL-3000: the integration of data reduction and structure solution--from diffraction images to an initial model in minutes. *Acta Crystallographica Section D Structural Biology* **2006,** (62), 859-866.

29.   Altomare, A.; Burla, M. C.; Camalli, M.; Carrozzini, B.; Cascarano, G.; Giacovazzo, C.; Guagliardi, A.; Moliterni, A. G. G.; Polidori, G.; Rizzi, A. C., EXPO: a program for full powder pattern decomposition and crystal structure solution. *J. Appl. Crystallogr.* **1999,** *32*, 339-340.

30.   Sheldrick, G. M.; Schneider, T. R., SHELXL : High-Resolution Refinement. *Macromol. Crystallogr. B* **1997**, 319-343.

31.   Farrugia, L. J., WinGX and ORTEP for Windows: an update. *J. Appl. Crystallogr.* **2012,** *45*, 849-854.

32.   Roisnel, T.; Rodriguez-Carjaval, J., A Window Tool for Powder Diffraction Patterns Analysis. *J. Mater. Sci. Forum* **2001,** *378* (3), 118-123.

33.   Kraus, W.; Nolze, G., POWDER CELL - A program for the representation and manipulation of crystal structures and calculation of the resulting X-ray powder patterns. *J. Appl. Crystallogr.* **1996,** *29*, 301-303.

34.   Le Bail, A., Monte Carlo Indexing with McMaille. *Powder Diffr.* **2004,** *19* (3), 249-254.

35.   Shinley, R. *The CRYSFIRE system for automatic powder indexing*.

36.   Wyszecki, G., Colorimetry. In *Handbook of Optics*, Driscoll, W. G.; Vaughan, W., Eds. Mac Graw-Hill Book Company: New-York, 1978; pp 1-15.

37.   CIE, *International Commission on Illumination - Technical report*. CIE: 1995; Vol. 13-3, p 16.

38.   Frisch, M. J.; Trucks, G. W.; Schlegel, H. B.; Scuseria, G. E.; Robb, M. A.; Cheeseman, J. R.; Scalmani, G.; Barone, V.; Mennucci, B.; Petersson, G. A.; Nakatsuji, H.; Caricato, M.; Li, X.; Hratchian, H. P.; Izmaylov, A. F.; Bloino, J.; Zheng, G.; Sonnenberg, J. L.; Hada, M.; Ehara, M.; Toyota, K.; Fukuda, R.; Hasegawa, J.; Ishida, M.; Nakajima, T.; Honda, Y.; Kitao, O.; Nakai, H.; Vreven, T.; Montgomery, J., J. A.; Peralta, J. E.; Ogliaro, F.; Bearpark, M.; Heyd, J. J.; Brothers, E.; Kudin, K. N.; Staroverov, V. N.; Kobayashi, R.; Normand, J.; Raghavachari; K.; Rendell, A.; Burant, J. C.; Iyengar, S. S.; Tomasi, J.; Cossi, M.; Rega, N.; Millam, N. J.; Klene, M.; Knox, J. E.; Cross, J. B.; Bakken, V.; Adamo, C.; Jaramillo, J.; Gomperts, R.; Stratmann, R. E.; Yazyev, O.; Austin, A. J.; Cammi, R.; Pomelli, C.; Ochterski, J. W.; Martin, R. L.; Morokuma, K.; Zakrzewski, V. G.; Voth, G. A.; Salvador, P.; Dannenberg, J. J.; Dapprich, S.; Daniels, A. D.; Farkas, Ö.; Foresman, J. B.; Ortiz, J. V.; Cioslowski, J.; Fox, D. J. *Gaussian 09, Revision A.02*, Gaussian Inc.: Wallingford, CT, 2009.

39.   Frisch, M. J.; Trucks, G. W.; Schlegel, H. B.; Scuseria, G. E.; Robb, M. A.; Cheeseman, J. R.; Scalmani, G.; Barone, V.; Mennucci, B.; Petersson, G. A.; Nakatsuji, H.; Caricato, M.; Li, X.; Hratchian, H. P.; Izmaylov, A. F.; Bloino, J.; Zheng, G.; Sonnenberg, J. L.; Hada, M.; Ehara, M.; Toyota, K.; Fukuda, R.; Hasegawa, J.; Ishida, M.; Nakajima, T.; Honda, Y.; Kitao, O.; Nakai, H.; Vreven, T.; Montgomery, J., J. A.; Peralta, J. E.; Ogliaro, F.; Bearpark, M.; Heyd, J. J.; Brothers, E.; Kudin, K. N.; Staroverov, V. N.; Kobayashi, R.; Normand, J.; Raghavachari; K.; Rendell, A.; Burant, J. C.; Iyengar, S. S.; Tomasi, J.; Cossi, M.; Rega, N.; Millam, N. J.; Klene, M.; Knox, J. E.; Cross, J. B.; Bakken, V.; Adamo, C.; Jaramillo, J.; Gomperts, R.; Stratmann, R. E.; Yazyev, O.; Austin, A. J.; Cammi, R.; Pomelli, C.; Ochterski, J. W.; Martin, R. L.; Morokuma, K.; Zakrzewski, V. G.; Voth, G. A.; Salvador, P.; Dannenberg, J. J.; Dapprich, S.; Daniels, A. D.; Farkas, Ö.; Foresman, J. B.; Ortiz, J. V.; Cioslowski, J.; Fox, D. J., Gaussian 09, Revision C.01. Inc., G., Ed. Gaussian Inc.: Wallingford, CT, 2009.

40.   Chai, J. D.; Head-Gordon, M., Long-Range Corrected Hybrid Density Functionals with Damped Atom-Atom Dispersion Corrections. *Phys. Chem. Chem. Phys.* **2008**, 6615-6620.

41.   Dexter, D. L., A theory of sensitized luminescence in solids. *J. Chem. Phys.* **1953,** *21* (5), 836-850.

42.   Förster, T., *Comparative effects of radiation*. John Wiley & Sons: New-York, 1960.

43.   Bünzli, J. C. G.; Eliseeva, S. V., Basics of lanthanide photophysics. In *Lanthanide Luminescence*, Hänninen, P.; Härmä, H., Eds. Springer Berlin Heidelberg: 2010; pp 1-45.

44.   Fourmigué, M., Halogen bonding: Recent advances. *Current Opin. Solid St. M.* **2009,** (13), 36-45.

45.   Cavallo, G.; Metrangolo, P.; Milani, R.; Pilati, T.; Priimagi, A.; Resnati, G.; Terraneo, G., The halogen bond. *Chem Rev* **2016,** (116), 2478-2601.

46.   Weissman, S. I., Intramolecular energy transfer - The fluorescence of complexes of europium. *J. Chem Phys* **1942,** *10* (4), 214-217.

47.   Shi, M.; Li, F.; Yi, T.; Zhang, D.; Hu, H.; Huang, C.-H., *Inorg. Chem.* **2005,** *44*, 8929.

48.   Prodi, L.; Maestri, M.; Ziessel, R.; Balzani, V., Luminescent Eu3+, Tb3+ and Gd3+ complexes of a branched triazacyclononane ligand containing three 2,2'bipyridine units. *Inorg. Chem.* **1991,** *30* (20), 3798-3802.

49.   Quici, S.; Cavazzini, M.; Marzanni, G.; Accors, i. G.; Armaroli, N.; Ventura, B.; Barigelletti, F., Visible and near-infrared luminescence from water soluble Lanthanide complexes. *Inorg. Chem.* **2005,** *44* (3), 529-537.

50.   Latva, M.; Takalo, H.; Mukkala, V.-M.; Matachescu, C.; Rodriguez-Ubis, J. C.; Kankare, J., Correlation between the lowest triplet state energy level of the ligand and lanthanide luminescence quantum yields. *J. Lumin.* **1997,** *75*, 149-169.

51.   Steemers, F. J.; Verboom, W.; Reinhoudt, D. N.; Van der Tol, E. B.; Verhoeven, J. W., New sensitizer-modified calix[4]arenes enabling Near-UV Excitation of complexed luminescent lanthanide ions. *J. Am. Chem. Soc.* **1995,** *117* (37), 9408-9414.

52.   Kasha, M., Characterization of electronic transitions in complex molecules. *Discuss. Faraday Soc.* **1950,** *9*, 14-19.

53.   Qian, H.; Cousins, M. E.; Horak, E. H.; Wakefield, A.; Liptak, M. D.; Aprahamian, I., Suppression of Kasha's rule as a mechanism for fluorescent molecular rotors and aggregation-induced emission. *Nat. Chem.* **2017,** (9), 83-87.

54.   Demchenko, A. P.; Tomin, V. I.; Chou, P. T., Breaking the Kasha Rule for More Efficient Photochemistry. *Chem Rev* **2017,** (117), 13353-13381.

55.   Fan, X.; Freslon, S.; Daiguebonne, C.; Le Polles, L.; Calvez, G.; Bernot, K.; Guillou, O., A family of lanthanide based coordination polymers with boronic acid as ligand. *Inorg. Chem.* **2015,** *54*, 5534-5546.

56.   Eliseeva, S. V.; Bünzli, J. C. G., Lanthanide luminescence for functionnal materials and bio-sciences. *Chem. Soc. Rev.* **2010,** *39* (1), 189-227.

57.   Suffren, Y.; Golessorkhi, B.; Zare, D.; Guénée, L.; Nozary, H.; Eliseeva, S. V.; Petoud, S.; Hauser, A.; Piguet, C., Taming lanthanide centered upconversion at the molecular level. *Inorg. Chem.* **2016,** *55* (20), 9964-9972.

58.   Zare, D.; Suffren, Y.; Guénée, L.; Eliseeva, S. V.; Nozary, H.; Aboshyan-Sorgho, L.; Petoud, S.; Hauser, A.; Piguet, C., Smaller than a nanoparticle with the desgn of discrete polynuclear molecular complexes displaying near-infrared to visible upconversion. *Dalton Trans.* **2015,** *44*, 2529-2540.

59.   Rodrigues, M. O.; Dutra, J. D. L.; Nunes, L. A. O.; de Sa, G. F.; de Azevedo, W. M.; Silva, P.; Paz, F. A. A.; Freire, R. O.; Junior, S. A., Tb3+->Eu3+ energy transferin mixed lanthanide organic frameworks. *J. Phys. Chem. C* **2012,** *116*, 19951-19957.

60.   Gao, M.-L.; Wang, W.-J.; Liu, L.; Han, Z.-B.; Wei, N.; Cao, X.-M.; Yuan, D.-Q., Microporous hexanuclear Ln(III) cluster-based metal-organic frameworks: color tunability for barcode applications ans selective removal of methylene blue. *Inorg. Chem.* **2017,** *56* (1), 511-517.

61.   Du, B.-B.; Zhu, Y.-X.; Pan, M.; Yue, M.-Q.; Hou, Y.-J.; Wu, K.; Zhang, L.-Y.; Chen, L.; Yin, S.-Y.; Fan, Y.-N.; Su, C. Y., Direct white light and dual-channel barcode module from Pr(III)-MOF crystals. *Chem. Comm.* **2015,** *51*, 12533-12536.

62.   Yang, Q. Y.; Pan, M.; Wei, S. C.; Li, K.; Du, B. B.; Su, C. Y., Linear dependance of photomuminescence in mixed Ln-MOFs for color tunabimity and barcode application. *Inorg. Chem.* **2015,** *54* (12), 5707-5716.

63.   White, K. A.; Chengelis, D. A.; Gogick, K. A.; Stehman, J.; Rosi, N. L.; Petoud, S., Near infra-red luminescent lanthanide MOF barcodes. *J. Am. Chem. Soc.* **2009,** *131* (50), 18069-18071.

GRAPHICAL ABSTRACT
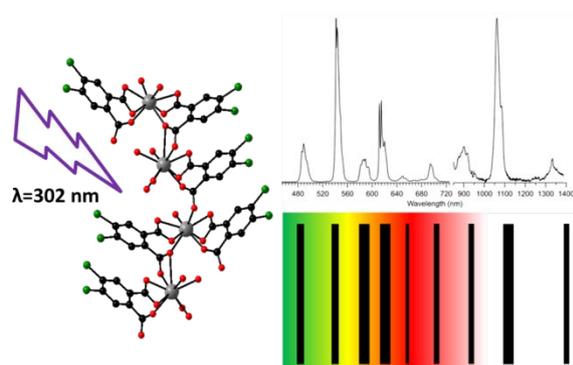
TOC SYNOPSYS

Reaction in water of 4,5-dichlorophthalate (dcpa^{2-}) with lanthanide ions leads to a family of isostructural homo- or hetero-lanthanide-based coordination polymers iso-structural with [Er$_2$(dcpa)$_3$(H$_2$O)$_5 \cdot$3H$_2$O]$_\infty$. Some of these compounds exhibit bright and highly tunable luminescence in both visible and infrared domains and could be of interest as far as luminescent bar-codes are targeted.